Dissipative hydrodynamics in 2 + 1 dimensions

A. K. Chaudhuri*
Variable Energy Cyclotron Centre, 1/AF, Bidhan Nagar, Kolkata 700 064, India
(Received 7 April 2006; published 5 October 2006)

In 2 + 1 dimensions, we simulated the hydrodynamic evolution of quark-gluon plasma (QGP) fluid with dissipation due to shear viscosity. Comparison of the evolution of ideal and viscous fluids, both initialized under the same conditions, e.g., same equilibration time, energy density and velocity profile, reveals that the dissipative fluid evolves slowly, cooling at a slower rate. Cooling slows even more at higher viscosities. The fluid velocities, however, evolve faster in a dissipative fluid than in an ideal fluid. The transverse expansion is also enhanced in dissipative evolution. For the same decoupling temperature, the freeze-out surface for a dissipative fluid is more extended than that for an ideal fluid. Dissipation produces entropy as a result of which particle production is increased. Particle production is increased as a result of the (i) the extension of the freeze-out surface and (ii) the change of the equilibrium distribution function to a nonequilibrium one, the latter effect being prominent at large transverse momentum. Compared to ideal fluid, transverse momentum distribution of pion production is considerably enhanced. Enhancement is greater at high p_T than at low p_T. Pion production also increases with viscosity; the greater the viscosity, the greater the pion production. Dissipation also modifies the elliptic flow, which is reduced in viscous dynamics. Also, contrary to ideal dynamics where elliptic flow continues to increase with transverse momentum, in viscous dynamics elliptic flow tends to saturate at large transverse momentum. The analysis suggests that the initial conditions of the hot, dense matter produced in Au+Au collisions at the Relativistic Heavy Ion Collider (RHIC), as extracted from ideal fluid analysis, can be changed significantly if the QGP fluid is viscous.

DOI: 10.1103/PhysRevC.74.044904 PACS number(s): 24.10.Nz, 47.75.+f, 25.75.Ld, 25.75.Nq

I. INTRODUCTION

Lattice quantum chromodynamics (QCD) predicts that under certain conditions (sufficiently high energy density and temperature) ordinary hadronic matter (where quarks and gluons are confined) can undergo a phase transition to a deconfined matter, commonly known as quark-gluon plasma (QGP). Nuclear physicists are trying to produce and detect this new phase of matter at the Relativistic Heavy Ion Collider (RHIC) at Brookhaven National Laboratory. Recent Au+Au collisions at RHIC indicate that dense, color opaque medium of deconfined matter is created in very central collisions [1–4]. It is now also understood that the quarks and gluons strongly interact, giving rise to the notion of sQGP (strongly interacting QGP). The experimental data have been successfully analyzed in an *ideal* fluid dynamic model [5]. Hydrodynamic evolution of ideal QGP, thermalized at $\tau_i = 0.6$ fm, with a central entropy density of 110 fm^{-3} or an energy density of 35 Gev/fm^3, can explain a large amount of the RHIC data, the p_T spectra of identified particles, the elliptic flow, etc. [5]. However, the experimental data do show deviation from ideal behavior. The ideal fluid description works well in almost central Au+Au collisions near midrapidity at top RHIC energy, but gradually breaks down in more peripheral collisions, at forward rapidity, or at lower collision energies [6], indicating the onset of dissipative effects. To quantitatively describe such deviations from ideal fluid dynamics requires the numerical implementation of *dissipative* relativistic fluid dynamics.

Eckart [7] and Landau and Lifshitz [8] formulated the theory of dissipative relativistic fluid. Their theories are called first-order theories and suffer from the problem of causality; the signal can travel faster than light. First-order theories assume that the entropy 4-current contains terms up to linear order in dissipative quantities. This restriction results in parabolic equations, which leads to a causality problem. The causality problem is removed in the second-order theories formulated by Israel and Stewart [9]. In second-order theories, dissipative fluxes are treated as (extended) thermodynamic variables and the linear relation between entropy 4-current and dissipative quantities is extended to include quadratic terms. The entropy 4-current contains terms up to second order in dissipative forces. The resulting equations are hyperbolic in nature and the causality problem is removed. Naturally second order theories are more complicated. In addition to the usual energy-momentum conservation equations, relaxation equations for dissipative fluxes are required to be solved simultaneously.

Though the theories of dissipative hydrodynamics [7–9] have been known for more than 30 years, significant progress toward their numerical implementation has only been made very recently [10–14]. Earlier attempts were restricted to simple one-dimensional Bjorken expansion [15]. Because the hot dense matter produced in RHIC collisions undergoes large transverse expansion, such models are not of much help in extracting the initial conditions of the fluid from the experiment. Recently Teaney [10] solved the hydrodynamic equations in a first-order dissipative theory. He used the blast wave model and calculated the corrections to thermal distribution functions considering shear viscosity only. Blast wave models lack dynamics. The freeze-out surface is parametrized and one

*Electronic address: akc@veccal.ernet.in

fits the freeze-out parameters with experimental observables. Information about the initial conditions of the hot dense matter is not available in blast wave models. In Refs. [12,13], second-order theories for dissipative fluid are solved for QGP fluid. Although the models are dynamic (energy-momentum conservation equations are solved), energy-momentum conservation equations are solved in 1+1 dimensions, assuming longitudinal boost-invariance and cylindrical symmetry. Thus these models do not give any information on the most sensitive experimental observable, the elliptic flow. In Ref. [14] explicit equations describing the space-time evolution of non-ideal relativistic fluid, undergoing boost-invariant longitudinal and arbitrary transverse expansion, are given. Equations are written for both first-order and second-order theories.

At the Variable Energy Cyclotron Centre, Kolkata, we developed a numerical code (AZHYDRO-KOLKATA) to solve both first-order and second-order dissipative hydrodynamics in $2+1$ dimensions. In this article we present AZHYDRO-KOLKATA results for first-order dissipative hydrodynamics. Results for second-order dissipative hydrodynamics will be presented in a later publication. As mentioned earlier, first-order theories are acausal; the signal can travel faster than light. In one dimension, first-order theories can be solved analytically. Analytical solutions indicate that early in the evolution, an unphysical reheating of the fluid can occur [12,16]. Even though in the present simulation we do not find any indication of early reheating, nevertheless we maintain that second-order results, which do not have the unphysical causality problem, are more reliable. In this paper we are concerned mainly with the effect of viscosity on fluid evolution and its effects on particle production, p_T distribution, and elliptic flow. No attempt is made to explain the experimental data.

This article is organized as follows: In Sec. II, we describe briefly the hydrodynamic equations needed for first-order dissipative hydrodynamics. In Sec. III, we describe the equation of state, the shear viscosity coefficient, and the initial conditions used in the present study. With dissipation, the equilibrium distribution function is changed. Corrections to equilibrium distribution function because of nonequilibrium effects are described in Sec. IV. We have studied particle (pion) production in the model. The relevant equations for pion production with the equilibrium distribution function and its correction due to nonequilibrium effects are discussed in Sec. V. Results of the numerical simulations are shown in Sec. VI. Finally, in Sec. VII, a summary is given and conclusions are drawn.

II. FIRST-ORDER DISSIPATIVE FLUID DYNAMICS

Relativistic dissipative hydrodynamics and associated equations in $2+1$ dimensions have been discussed in detail in Ref. [14]. Any fluid dynamical approach starts from the conservation laws for the conserved charges and for energy momentum. For a singly charged fluid, the conservation laws are

$$\partial_\mu N^\mu = 0 \tag{2.1}$$

$$\partial_\mu T^{\mu\nu} = 0. \tag{2.2}$$

It must also ensure the second law of thermodynamics

$$\partial_\mu S^\mu \geqslant 0, \tag{2.3}$$

where S^μ is the entropy current.

In the present article we restrict ourselves to the central rapidity region, where the QGP fluid is essentially baryon-free. We thus neglect Eq. (2.1). To keep the calculations simple, we consider the most important dissipative term, shear viscosity, and neglect the other dissipative terms, e.g., heat conduction and bulk viscosity. For a baryon-free fluid, the heat conduction is zero. The bulk viscosity is zero for QGP (point particles). The bulk viscosity will be nonzero in the hadronic phase but presently we neglect it.

With the help of hydrodynamic 4-velocity u^μ (normalized as $u^\mu u_\mu = 1$) and projector $\Delta^{\mu\nu} = g^{\mu\nu} - u^\mu u^\nu$, with only shear viscosity as the dissipative flux, in Landau's frame, the energy momentum tensor and the entropy 4-current, can be decomposed as

$$T^{\mu\nu} = T^{\mu\nu}_{\rm eq} + \delta T^{\mu\nu} = \varepsilon\, u^\mu u^\nu - p\Delta^{\mu\nu} + \pi^{\mu\nu} \tag{2.4}$$

$$S^\mu = S^\mu_{\rm eq} + \delta S^\mu = s\, u^\mu + \Phi^\mu, \tag{2.5}$$

where $\varepsilon = u_\mu T^{\mu\nu} u_\nu$ is the energy density; p is the local pressure; $\pi^{\mu\nu}$ is the non-ideal part of the energy-momentum tensor, the stress tensor due to shear viscosity; $s = u_\mu S^\mu$ is the entropy density; and Φ^μ is the entropy flux due to dissipation.

In the first-order theories, the shear stress tensor is written as

$$\pi^{\mu\nu} = 2\eta \nabla^{\langle\mu} u^{\nu\rangle}, \tag{2.6}$$

where η is the shear viscosity coefficient and $\nabla^{\langle\mu} u^{\nu\rangle}$ is a traceless symmetric tensor defined as

$$\nabla^{\langle\mu} u^{\nu\rangle} = \left[\tfrac{1}{2}(\Delta^{\mu\sigma}\Delta^{\nu\tau} + \Delta^{\nu\sigma}\Delta^{\mu\tau}) - \tfrac{1}{3}\Delta^{\mu\nu}\Delta^{\sigma\tau}\right]. \tag{2.7}$$

Viscous pressure $\pi^{\mu\nu}$ is symmetric ($\pi^{\mu\nu} = \pi^{\nu\mu}$), traceless ($\pi^\mu_\mu = 0$), and transverse to hydrodynamic velocity ($u_\mu \pi^{\mu\nu} = 0$). The 16-component $\pi^{\mu\nu}$ has only 5 independent components. As mentioned in the beginning, we have solved the equations with the assumption of longitudinal boost-invariance. With boost-invariance the number of independent shear stress tensors further reduces to 3.

Heavy ion collisions are best described in terms of proper time $\tau = \sqrt{t^2 - z^2}$ and rapidity $\eta_s = \frac{1}{2}\ln\frac{t+z}{t-z}$ (we use the subscript s to distinguish spatial rapidity from the viscous coefficient η). In (τ, x, y, η_s) coordinates, with longitudinal boost-invariance, the hydrodynamic 4-velocity can be written as

$$\begin{aligned} u^\mu &= (u^\tau, u^x, u^y, u^{\eta_s}) \\ &= (\gamma_\perp, \gamma_\perp v_x, \gamma_\perp v_y, 0), \end{aligned} \tag{2.8}$$

with

$$\gamma_\perp = 1/\sqrt{1 - v_x^2 - v_y^2}.$$

Explicit equations for energy-momentum conservation in the (τ, x, y, η_s) coordinate system were developed in Ref. [14]. Here we rewrite the results in a form suitable for numerical algorithm. The energy-momentum conservation

equations are

$$\partial_\tau(\tilde{T}^{\tau\tau}) + \partial_x(\tilde{T}^{\tau\tau}\overline{v}_x) + \partial_y(\tilde{T}^{\tau\tau}\overline{v}_y) = -(p + \tau^2\pi^{\eta\eta}), \quad (2.9)$$

$$\partial_\tau(\tilde{T}^{\tau x}) + \partial_x(\tilde{T}^{\tau x}v_x) + \partial_y(\tilde{T}^{\tau x}v_y) = -\partial_x(\tilde{p} + \tilde{\pi}^{xx} - \tilde{\pi}^{\tau x}v_x) - \partial_y(\tilde{\pi}^{xy} - \tilde{\pi}^{\tau x}v_y), \quad (2.10)$$

$$\partial_\tau(\tilde{T}^{\tau y}) + \partial_x(\tilde{T}^{\tau y}v_x) + \partial_y(\tilde{T}^{\tau y}v_y) = -\partial_x(\tilde{\pi}^{xy} - \tilde{\pi}^{\tau y}v_x) - \partial_y(\tilde{p} + \tilde{\pi}^{yy} - \tilde{\pi}^{\tau y}v_y), \quad (2.11)$$

where $\overline{v}_x = T^{\tau x}/T^{\tau\tau}$ and $\overline{v}_y = T^{\tau y}/T^{\tau\tau}$. We have used the notation "tilde" to represent quantities multiplied by the factor τ, $\tilde{p} = \tau p$ and similarly $\tilde{T}^{ij} = \tau T^{ij}$. We note that, unlike in ideal fluid, in viscous fluid dynamics conservation equations contain additional pressure gradients containing the dissipative fluxes. Both $T^{\tau x}$ and $T^{\tau y}$ components of energy-momentum tensors now evolve under the influence of additional pressure gradients.

In first-order theory, the shear stress tensor components required in the preceding equations are

$$\pi^{\tau x} = 2\eta\left[-\frac{1}{2}\partial_x\gamma_\perp + \frac{1}{2}\partial_\tau(\gamma_\perp v_x) - \frac{1}{2}D\left(\gamma_\perp^2 v_x\right) + \frac{\theta}{3}\gamma_\perp^2 v_x\right], \quad (2.12)$$

$$\pi^{\tau x} = 2\eta\left[-\frac{1}{2}\partial_y\gamma_\perp + \frac{1}{2}\partial_\tau(\gamma_\perp v_y) - \frac{1}{2}D(\gamma_\perp^2 v_y) + \frac{\theta}{3}\gamma_\perp^2 v_y\right], \quad (2.13)$$

$$\pi^{\tau\tau} = 2\eta\left[\frac{\theta}{3}(\gamma_\perp^2 - 1) + \partial_\tau\gamma_\perp - \frac{1}{2}D(\gamma_\perp^2)\right], \quad (2.14)$$

$$\pi^{\eta\eta} = 2\eta\left[\frac{1}{\tau^2}\left(\frac{\theta}{3} - \frac{\gamma_\perp}{\tau}\right)\right], \quad (2.15)$$

$$\pi^{xx} = 2\eta\left[-\partial_x(\gamma_\perp v_x) - \frac{1}{2}D(\gamma_\perp^2) + \frac{\theta}{3}\left(1 + \gamma_\perp^2 v_x^2\right)\right], \text{ and} \quad (2.16)$$

$$\pi^{yy} = 2\eta\left[-\partial_x(\gamma_\perp v_y) - \frac{1}{2}D(\gamma_\perp^2) + \frac{\theta}{3}\left(1 + \gamma_\perp^2 v_y^2\right)\right], \quad (2.17)$$

where $D = u^\mu\partial_\mu$ is the convective time derivative,

$$D = \gamma_\perp(\partial_\tau + v_x\partial_x + v_y\partial_y), \quad (2.18)$$

and θ is the local expansion rate, given by

$$\theta = \frac{\gamma_\perp}{\tau} + \partial_\tau\gamma_\perp + \partial_x(v_x\gamma_\perp) + \partial_y(v_y\gamma_\perp). \quad (2.19)$$

Given an equation of state, if energy density (ε) and fluid velocity (v_x and v_y) distributions at any time τ_i are known, Eqs. (2.9)–(2.10) can be integrated to obtain ε, v_x, and v_y at the next time step τ_{i+1}. Whereas for ideal hydrodynamics this procedure works perfectly, viscous hydrodynamics poses a problem in that shear stress tensor components contain time derivatives, $\partial_\tau\gamma_\perp$, $\partial_\tau u^x$, $\partial_\tau u^x$, etc. Thus, at time step τ_i one needs the still unknown time derivatives. Numerically, the time derivatives at step τ_i could be obtained if the velocities at time steps τ_i and τ_{i+1} were known. One possible way to circumvent the problem is to use the time derivatives of the previous step; i.e., use the velocities at time steps τ_{i-1} and τ_i to calculate the derivatives at time step τ_i [13]. In first-order theories, this problem is circumvented by calculating the time derivatives from the ideal equations of motion

$$Du^\mu = \frac{\nabla^\mu p}{\varepsilon + p}, \quad (2.20)$$

$$D\varepsilon = -(\varepsilon + p)\nabla_\mu u^\mu. \quad (2.21)$$

With the help of these two equations all the time derivatives can be expressed entirely in terms of spatial gradients [10,17]. First-order theories are restricted to contain terms at most linear in dissipative quantities. Neglect of viscous terms can contribute only in second-order corrections, which are neglected in first-order theories.

III. EQUATION OF STATE, VISCOSITY COEFFICIENT AND INITIAL CONDITIONS

A. Equation of state

One of the most important inputs of a hydrodynamic model is the equation of state. Through this input macroscopic hydrodynamic models make contact with the microscopic world. In the present calculation we use the equation of state, EOS-Q, developed in Ref. [5]. It is a two-phase equation of state. The hadronic phase of EOS-Q is modeled as a non-interacting gas of hadronic resonance. As the temperature is increased, larger and larger fractions of available energy go into production of heavier and heavier resonances. This results in a soft equation of state, with small speed of sound, $c_s^2 \approx 0.15$. With increasing temperature, the available volume is filled up with resonances and the hadronic states start to overlap, and microscopic degrees of freedom are changed from hadrons to deconfined quarks and gluons. The QGP phase is modeled as a non-interacting quark (u, d, and s) and gluons, confined by a bag pressure B. The corresponding equation of state, $p = \frac{1}{3}e - \frac{4}{3}B$, is stiff with a speed of sound $c_s^2 = \frac{1}{3}$. The two phases are matched by Maxwell construction at the critical temperature $T_c = 164$ MeV, adjusting the bag pressure $B^{1/4} = 230$ MeV. As discussed in Ref. [5], ideal hydrodynamics explains a large amount of RHIC Au+Au data with EOS-Q.

B. Shear viscosity coefficient

The shear viscosity coefficient (η) of dense QGP or resonance hadron gas is quite uncertain. In a perturbative regime, the shear viscosity of QGP is estimated [18,19] as

$$\eta = 86.473\frac{1}{g^4}\frac{T^3}{\log g^{-1}}. \quad (3.1)$$

With entropy of QGP, $s = 37\frac{\pi^2}{15}T^3$ and $\alpha_s \approx 0.5$, the ratio of viscosity over the entropy in the perturbative regime is estimated as

$$\left(\frac{\eta}{s}\right)_{\text{pert}} \approx 0.135. \quad (3.2)$$

However, QGP produced in nuclear collisions is nonperturbative. It is strongly interacting QGP. Recently, using the ADS/CFT correspondence [20,21], the shear viscosity of a strongly coupled gauze theory, N = 4 SUSY YM, was evaluated, $\eta = \frac{\pi}{8} N_c^2 T^3$, and the entropy was given by $s = \frac{\pi^2}{2} N_c^2 T^3$. Thus in the strongly coupled field theory

$$\left(\frac{\eta}{s}\right)_{\mathrm{ADS/CFT}} = \frac{1}{4\pi} \approx 0.08, \tag{3.3}$$

which is approximately two times smaller than the perturbative estimate. In the present article, we treat the shear viscosity as a parameter of the model. To demonstrate the effect of viscosity on flow and subsequent particle production, we use both the perturbative and the ADS/CFT estimate of viscosity.

First-order theories are acausal. As mentioned earlier, unphysical effects, such as reheating of the fluid, can occur early in the evolution. In one dimension the energy-momentum conservation equation can be solved analytically. If the initial fluid temperature is T_i at initial time τ_i, for constant η/s, the fluid temperature at time τ can be obtained as [16]

$$T(\tau) = T_i \left(\frac{\tau_i}{\tau}\right)^{1/3} \left[1 + \frac{2}{3\tau_i T_i} \frac{\eta}{s} \left(1 - \left(\frac{\tau_i}{\tau}\right)^{2/3}\right)\right]. \tag{3.4}$$

For early times, $\tau < \tau_{\max}$,

$$\tau_{\max} = \tau_i \left(\frac{1}{3} + \frac{s}{\eta} \frac{\tau_i T_i}{2}\right)^{-3/2}, \tag{3.5}$$

the solution shows an unphysical reheating. The unphysical reheating is minimized if $\tau_{\max}$ is small or $\eta/s \ll \tau_i T_i$. As is explained below, we used an initial time, $\tau_i = 0.6$ fm/c, and an initial temperature of the fluid, $T_i = 0.35$ GeV. For both the values of viscosity, $\eta/s \ll \tau_i T_i$, the unphysical reheating is minimized.

Shear viscosity can also be expressed in terms of sound attenuation length, Γ_s, defined as

$$\Gamma_s = \frac{\frac{4\eta}{3}}{sT}. \tag{3.6}$$

Γ_s is equivalent to the mean free path and for a valid hydrodynamic description $\Gamma_s/\tau \ll 1$; i.e., the mean free path is much less than the system size. With the present choice of equilibration time and temperature, for both the ADS/CFT and the perturbative estimate of viscosity, at initial time, Γ_s/τ is much less than unity and hydrodynamics remains a valid description. At a later time the validity condition becomes even better.

C. Initial conditions

As discussed earlier, ideal hydrodynamics has been very successful in explaining a large amount of data in RHIC 200A GeV Au+Au collisions [5]. In the present demonstrative calculations, we use initial conditions similar to those used in Ref. [5]. Details of the initial conditions can be found in Ref. [5]. Note that in Ref. [5], the initial transverse energy is parametrized geometrically. At an impact parameter $\vec{b}$, transverse distribution of wounded nucleons $N_{\mathrm{WN}}(x, y, \vec{b})$ and of binary NN collisions $N_{\mathrm{BC}}(x, y, \vec{b})$ are calculated in a Glauber model. A collision at impact parameter $\vec{b}$ is assumed to contain 25% hard scattering (proportional to the number of binary collisions) and 75% soft scattering (proportional to the number of wounded nucleons). The transverse energy density profile at impact parameter $\vec{b}$ is then obtained as

$$\varepsilon(x, y, \vec{b}) = \varepsilon_0(0.75 \times N_{\mathrm{WN}}(x, y, \vec{b}) + 0.25 \times N_{\mathrm{BC}}(x, y, \vec{b})). \tag{3.7}$$

The parameter ε_0 and the initial equilibration time τ_i are fixed to reproduce the experimental transverse momentum distribution of pions in central Au+Au collisions. STAR and PHENIX data are fitted to obtain an initial equilibrium time of $\tau_i = 0.6$ fm and a central entropy density of $s = 110\ \mathrm{fm}^{-3}$. This corresponds to energy density of the fluid as 25 GeV/fm^3 or an initial temperature of 350 MeV. Apart from the initial energy density, the initial velocity distribution is also required in hydrodynamic calculations. In the present calculation it is assumed that the at the initial time τ_i fluid velocities are zero, $v_x(x, y) = v_y(x, y) = 0$.

In dissipative hydrodynamics, additionally, the initial conditions for the dissipative fluxes must be specified. In the present article we assume that by the equilibration time τ_i, the dissipative fluxes have attained their longitudinal boost-invariant values.

$$\pi^{\tau x} = 0 \tag{3.8}$$

$$\pi^{\tau x} = 0 \tag{3.9}$$

$$\pi^{\tau\tau} = 0 \tag{3.10}$$

$$\tau^2 \pi^{\eta\eta} = -4\eta/\tau_i \tag{3.11}$$

$$\pi^{xx} = 2\eta/\tau_i \tag{3.12}$$

$$\pi^{yy} = 2\eta/\tau_i \tag{3.13}$$

IV. NONEQUILIBRIUM DISTRIBUTION FUNCTION

With dissipation the system is not in equilibrium and the equilibrium distribution function

$$f^{(0)}(x, p) = \frac{1}{\exp[\beta(u_\mu p^\mu - \mu)] \pm 1}, \tag{4.1}$$

with inverse temperature $\beta = 1/T$ and chemical potential μ, can no longer describe the system. In a highly nonequilibrium system, the distribution function is unknown. If the system is slightly off-equilibrium, then it is possible to calculate correction to the equilibrium distribution function due to (small) nonequilibrium effects. The slightly off-equilibrium distribution function can be approximated as

$$F(x, p) = f^{(0)}(x, p)[1 + \phi(x, p)], \tag{4.2}$$

$\phi(x, p)$ is the deviation from the equilibrium distribution function $f^{(0)}$. With shear viscosity as the only dissipative forces $\phi(x, p)$ can be locally approximated by a quadratic function of 4-momentum,

$$\phi(x, p) = \varepsilon_{\mu\nu} p^\mu p^\nu. \tag{4.3}$$

Without any loss of generality $\varepsilon_{\mu\nu}$ can be written as

$$\varepsilon_{\mu\nu} = C\pi^{\mu\nu}, \quad C = \frac{\beta^2}{2(\varepsilon + p)}, \tag{4.4}$$

completely specifying the nonequilibrium distribution function.

V. PARTICLE SPECTRA

With the nonequilibrium distribution function thus specified, it can be used to calculate the particle spectra from the freeze-out surface. In the standard Cooper-Frye prescription, particle distribution is obtained as

$$E\frac{dN}{d^3p} = \frac{dN}{dyd^2p_T} = \int_\Sigma d\Sigma_\mu p^\mu f(x,p). \tag{5.1}$$

In (τ, x, y, η_s) coordinate, the freeze-out surface is parametrized as

$$\Sigma^\mu = (\tau_f(x,y)\cosh\eta_s, x, y, \tau_f(x,y)\sinh\eta_s). \tag{5.2}$$

and the normal vector on the hyper surface is

$$d\Sigma_\mu = \left(\cosh\eta_s, -\frac{\partial\tau_f}{\partial x_f}, -\frac{\partial\tau_f}{\partial y_f}, -\sinh\eta_s\right)\tau_f dxdyd\eta_s. \tag{5.3}$$

At the fluid position (τ, x, y, η_s) the particle 4-momenta are parametrized as

$$p^\mu = (m_T\cosh(\eta_s - Y), p^x, p^y, m_T\sinh(\eta_s - Y)). \tag{5.4}$$

The volume element $p^\mu d\Sigma_\mu$ becomes

$$p^\mu d\Sigma_\mu = (m_T\cosh(\eta - Y) - \vec{p}_T.\vec{\nabla}_T\tau_f)\tau_f dxdyd\eta. \tag{5.5}$$

The equilibrium distribution function involves the term $p^\mu u_\mu/T$ which can be evaluated as

$$\frac{p^\mu u_\mu}{T} = \frac{\gamma(m_T\cosh(\eta - Y) - \vec{v}_T.\vec{p}_T - \mu/\gamma)}{T}. \tag{5.6}$$

The nonequilibrium distribution function requires the sum $p^\mu p^\nu \pi_{\mu\nu}$

$$p_\mu p_\nu \pi^{\mu\nu} = a_1\cosh^2(\eta - Y) + a_2\cosh(\eta - Y) + a_3, \tag{5.7}$$

with

$$a_1 = m_T^2(\pi^{\tau\tau} + \tau^2\pi^{\eta\eta}) \tag{5.8}$$

$$a_2 = -2m_T(p_x\pi^{\tau x} + p_y\pi^{\tau y}) \tag{5.9}$$

$$a_3 = p_x^2\pi^{xx} + p_y^2\pi^{yy} + 2p_xp_y\pi^{xy} - m_T^2\tau^2\pi^{\eta\eta}. \tag{5.10}$$

Inserting all the relevant formulas in Eq. (5.1) and integrating over spatial rapidity one obtains

$$\frac{dN}{dyd^2p_T} = \frac{dN^{\rm eq}}{dyd^2p_T} + \frac{dN^{\rm neq}}{dyd^2p_T}, \tag{5.11}$$

with

$$\frac{dN^{\rm eq}}{dyd^2p_T} = \frac{g}{(2\pi)^3}\int dxdy\tau_f[m_TK_1(n\beta) - p_T\vec{\nabla}_T\tau_fK_0(n\beta)] \tag{5.12}$$

$$\frac{dN^{\rm neq}}{dyd^2p_T} = \frac{g}{(2\pi)^3}\int dxdy\tau_f\left[m_T\left\{\frac{a_1}{4}K_3(n\beta) + \frac{a_2}{2}K_2(n\beta) + \left(\frac{3a_1}{4} + a_3 + 1\right)K_1(n\beta) + \frac{a_2}{2}K_0(n\beta)\right\}\right.$$
$$\left. - \vec{p}_T.\vec{\nabla}_T\tau_f\left\{\frac{a_1}{2}K_2(n\beta) + a_2K_1(n\beta) + \left(\frac{a_1}{2} + a_3 + 1\right)K_0(n\beta)\right\}\right], \tag{5.13}$$

where K_0, K_1, K_2, and K_3 are the modified Bessel functions.

We also show results for elliptic flow v_2. It is defined as

$$V_2 = \frac{\int_0^{2\pi}\frac{dN}{dyd^2p_T}\cos(2\phi)d\phi}{\int_0^{2\pi}\frac{dN}{dyd^2p_T}d\phi}. \tag{5.14}$$

VI. RESULTS

A. Evolution of the viscous fluid

The energy-momentum conservation equations (2.9)–(2.11) are solved using the SHASTA-FCT algorithm. We have made extensive changes to the publicly available code AZHYDRO (described in [5]) for simulation of ideal fluid. The modified code, called AZHYDRO-KOLKATA, simulates the evolution of dissipative fluid in both first- and second-order theory. In this section we present results obtained using AZHYDRO-KOLKATA for the first-order theory of dissipative fluid. Below we show the results obtain in a Au+Au collision at impact parameter $b = 6.8$ fm, which approximately corresponds to 16%–24% centrality Au+Au collisions. With the same initial conditions, we solve the energy-momentum conservation equations for ideal fluid and viscous fluid.

In Fig. 1, we show the constant energy density contour plot in the x-y plane after an evolution of 5 fm. The black lines represent ideal fluid evolution. The red and blue lines represent viscous fluid with ADS/CFT ($\eta/s = 0.08$) and perturbative ($\eta/s = 0.135$) estimates of viscosity. Constant energy density contours, as depicted in Fig. 1, indicate that with viscosity fluid cools slowly. Cooling gets slower as viscosity increases. Thus at any point in the x-y plane, the viscous fluid temperature

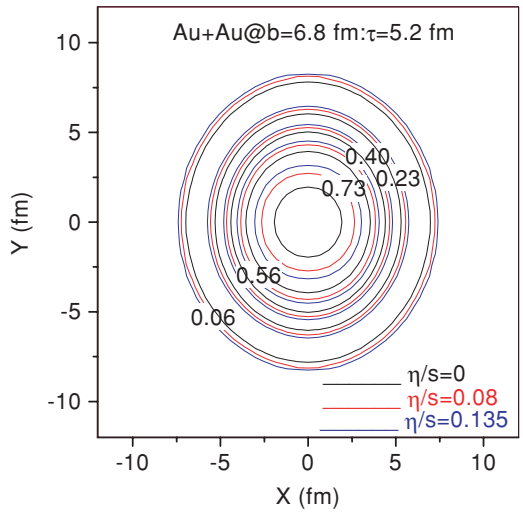

FIG. 1. (Color online). Contour plots of energy density at (proper) time $\tau = 5.6$ fm. The black lines represent ideal fluid ($\eta/s = 0$). The red and blue lines represent, respectively, viscous fluid with ADS/CFT ($\eta/s = 0.08$) and perturbative ($\eta/s = 0.135$) estimates of viscosity.

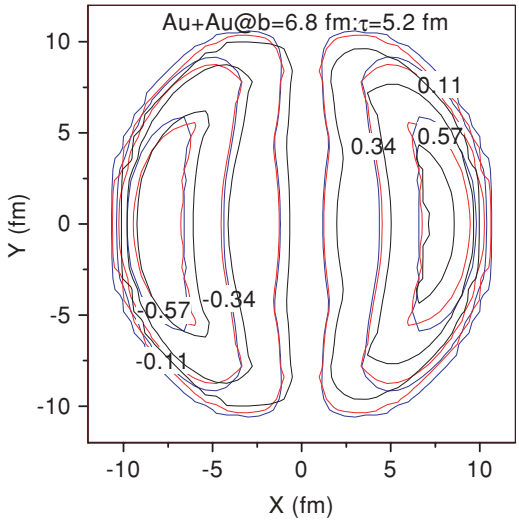

FIG. 2. (Color online). Contour plots of x component of fluid velocity v_x at $\tau = 5.6$ fm. The black lines represent ideal fluid ($\eta/s = 0$). The red and blue lines represent viscous fluid with ADS/CFT and perturbative estimates of viscosity, $\eta/s = 0.08$ and 0.135, respectively.

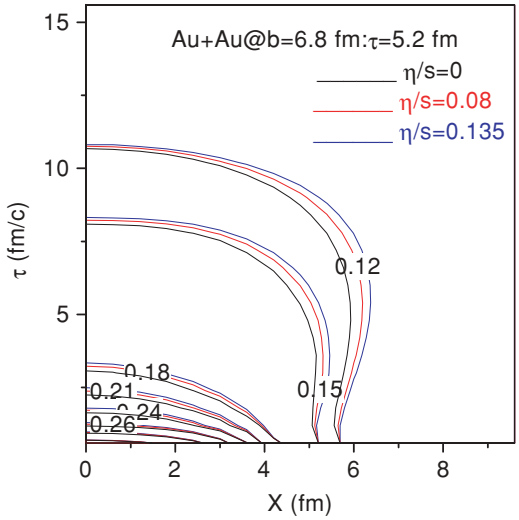

FIG. 3. (Color online). Contour plots of temperature at $y = 0$ fm in the x-τ plane. The black lines represent ideal fluid ($\eta/s = 0$). The red and blue lines represent viscous fluid with $\eta/s = 0.08$ and 0.135, respectively.

is higher than that of the ideal fluid. The results are in accordance with our expectations. So for dissipative fluid, the ideal equation of motion, Eq. (2.21), is changed to

$$D\varepsilon = -(\varepsilon + p)\nabla_\mu u^\mu + \pi^{\mu\nu}\nabla_{\langle\mu}u_{\nu\rangle}. \tag{6.1}$$

Because of viscosity, the evolution of energy density is slowed down.

In Fig. 2, we show the constant v_x contour plot in the x-y plane again at $\tau = 5.6$ fm. As before the black lines represent the ideal fluid evolution. The red and blue lines represent viscous fluid with $\eta/s = 0.08$ and 0.135, respectively. In the central region of the fluid, the viscous fluid has more velocity than its ideal counterpart. With viscosity, while the energy density evolves slowly, the fluid velocity evolves faster. The contour plot of the y component of fluid velocity also indicates similar results.

To obtain an idea of the transverse expansion of viscous fluid, as opposed to ideal fluid, in Fig. 3 we show the constant temperature contours in the τ-x plane, at a fixed value of $y = 0$ fm. Transverse expansion is substantially enhanced in a viscous fluid. The greater the viscosity is, the greater transverse expansion. The plot also indicates that at late time, fluid at $x = y = 0$ behaves similarly to the ideal fluid.

First order dissipative theories are acausal. As mentioned earlier, acausality can lead to unphysical behavior such as reheating of the fluid in the early stage of evolution [12,16]. Do we see any reheating? In Fig. 4, the evolution of temperature in viscous dynamics with a perturbative estimate of viscosity ($\eta/s = 0.135$) is shown. We have shown the temperature at two positions of the fluid, $x = y = 0$ (the solid line) and $x = 0$, $y = 3$ fm (the dashed line). In both positions of the fluid, with time, as the fluid expands the temperature decreases (as it should be). We find no evidence of reheating. Reheating is not seen also with the ADS/CFT estimate of viscosity.

In Fig. 5, we show shear stress tensors $\pi^{\tau\tau}(x, y = 0)$, $\tau^2\pi^{\eta\eta}(x, y = 0)$, $\pi^{xx}(x, y = 0)$, and $\pi^{yy}(x, y = 0)$ as a function of x. $\eta/s = 0.135$. The solid, long-dashed, dashed, and short-dashed lines are for times 0.6, 2.2, 3.2, and 4.2 fm, respectively. Initially at $\tau = 0.6$ fm, $\pi^{\tau\tau}$ is zero. As the fluid evolves, $\pi^{\tau\tau}$ increases rapidly to a maximum and then decreases. By 4 fm of evolution, it decreases to very small values. We also note that $\pi^{\tau\tau}$ is never very large. The viscous pressures $\tau^2\pi^{\eta\eta}$, π^{xx}, and π^{yy} are nonzero at initial time $\tau_i = 0.6$ fm. As the fluid evolves, these viscous fluxes rapidly decrease to very small values.

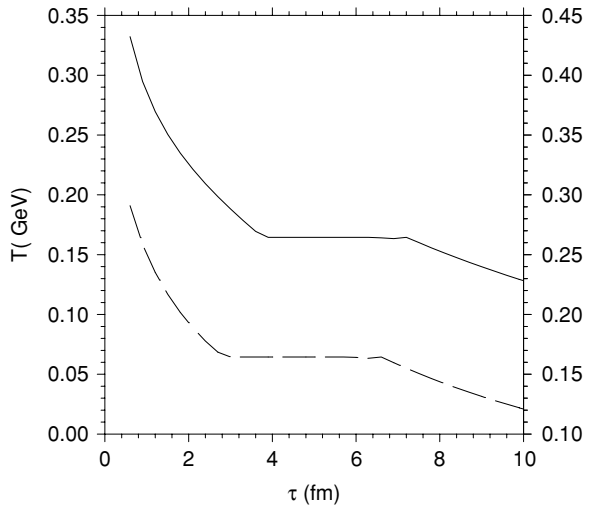

FIG. 4. Evolution of the temperature in viscous dynamics with a perturbative estimate of viscosity, $\eta/s = 0.135$. The solid and dashed lines represent fluid at $x = y = 0$ and $x = 0$, $y = 3$ fm, respectively. The $x = 0$, $y = 3$ fm curve is plotted using the right-side scale.

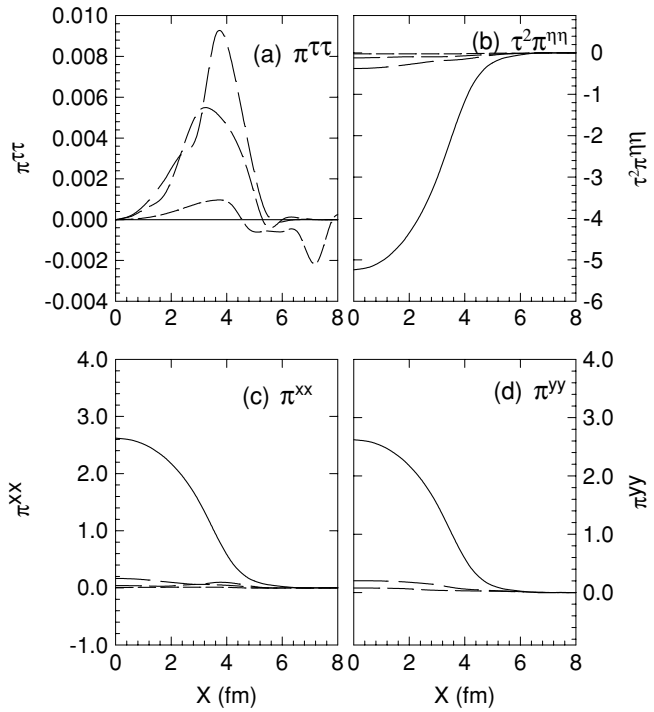

FIG. 5. Shear stress tensors $\pi^{\tau\tau}(x, y = 0)$, $\tau^2\pi^{\eta\eta}(x, y = 0)$, $\pi^{xx}(x, y = 0)$, and $\pi^{yy}(x, y = 0)$ at $\tau = 0.6$, 2.2, 3.2, and 4.2 fm. The solid, long-dashed, dashed, and short-dashed lines are for times 0.6, 2.2, 3.2, and 4.2 fm, respectively.

Viscosity generates entropy. In the model entropy generation due to dissipation can be calculated as

$$\partial_\mu S^\mu = \frac{\pi^{\mu\nu}\pi_{\mu\nu}}{2\eta T}. \tag{6.2}$$

The evolution of spatially average entropy is shown in Fig. 6. Entropy generation saturates after ∼2 fm of evolution. It is expected. As seen in Fig. 5, viscous fluxes rapidly decrease and by 2 fm of evolution, the viscous fluxes are decreased sufficiently and do not contribute significantly to the entropy.

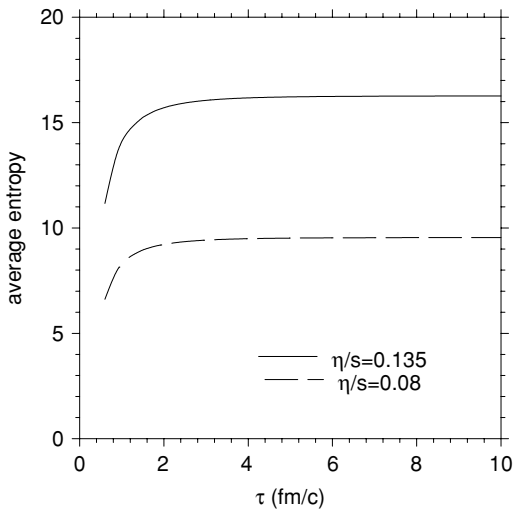

FIG. 6. Evolution of average entropy with proper time for two values of η/s.

B. Particle spectra

In these exploratory calculations we do not attempt to fit experimental data. We just exhibit the effect of viscosity on (i) the transverse momentum distribution and (ii) the elliptic flow of pions. Viscosity influences the particle production by (i) changing the freeze-out surface (freeze-out surface is extended) and (ii) introducing a correction to the equilibrium distribution function. Nonequilibrium correction to the equilibrium distribution function depends, quadratically on the momentum and linearly on the viscous fluxes.

In Fig. 7, we show the transverse momentum distribution of pions obtained in the Cooper-Frye formalism. Freeze-out temperature is $T_F = 0.158$ GeV. In this calculation, resonance contribution to pion spectra is neglected. Pion production is increased in viscous dynamics. We also note that the effect of viscosity is more prominent at large p_T than at low p_T. p_T spectra of pions are flattened with viscosity. Particle production increases if viscosity increases. With the ADS/CFT estimate of viscosity, $\eta/s = 0.08$, at $p_T = 3$ GeV, pion production is increased by a factor 3, whereas with the perturbative estimate of viscosity, $\eta/s = 0.135$, the production is increased by a factor of 5. The increase is even greater at larger p_T.

We obtained the nonequilibrium distribution as a correction to the equilibrium distribution function. It is implied that nonequilibrium effects are small and the ratio

$$\frac{dN^{\text{neq}}}{dN^{\text{eq}}} = \frac{\frac{dN^{\text{neq}}}{dyd^2p_T}}{\frac{dN^{\text{eq}}}{dyd^2p_T}} \tag{6.3}$$

is less than 1. In Fig. 8, the ratio is shown as a function of p_T. With the ADS/CFT estimate of viscosity, $\eta/s = 0.08$, the nonequilibrium correction to particle production becomes

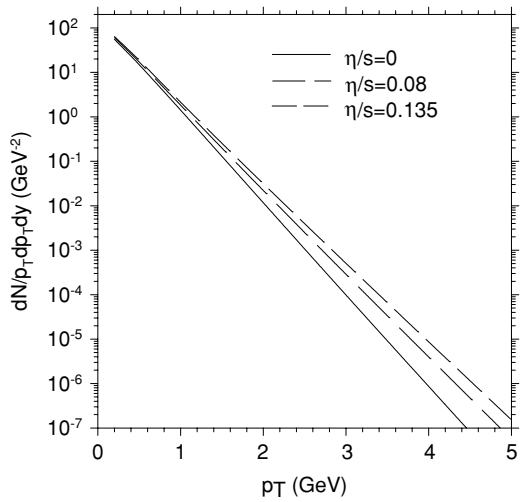

FIG. 7. P_T distribution of pions. The solid line represents the ideal fluid. The long-dashed and medium-dashed lines represent the viscous fluid with ADS/CFT ($\eta/s = 0.08$) and perturbative ($\eta/s = 0.135$) estimates of viscosity. The nonequilibrium correction to the equilibrium distribution function is included.

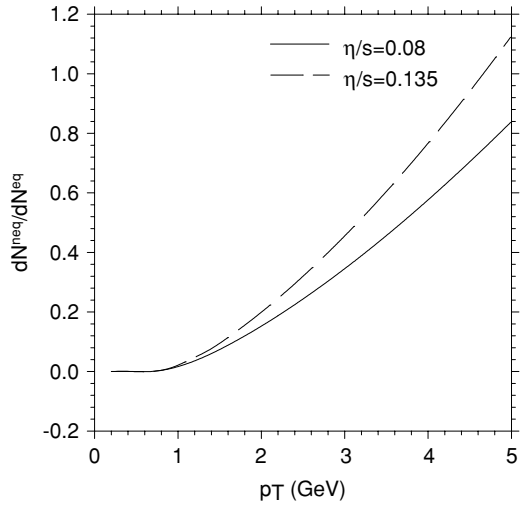

FIG. 8. Ratio of correction to particle production due to nonequilibrium distribution to equilibrium distribution function.

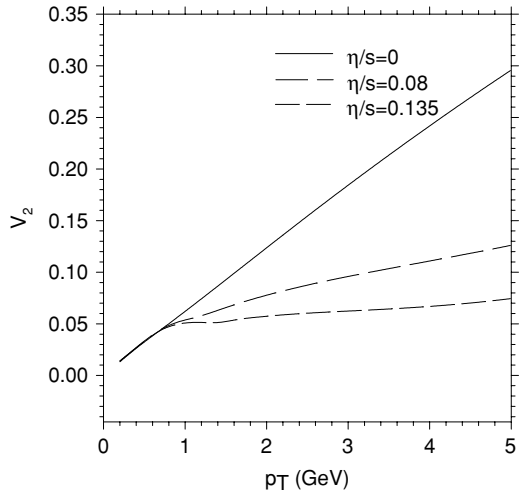

FIG. 9. Elliptic flow as a function of transverse momentum. The solid line represents the ideal fluid. The long-dashed and medium-dashed lines represents the viscous fluid with $\eta/s = 0.08$ and 0.135, respectively. Nonequilibrium correction to equilibrium distribution function is included.

comparable to the equilibrium contribution beyond $p_T = 5$ GeV. However, with the perturbative estimate, $\eta/s = 0.135$, the nonequilibrium correction becomes comparable to or exceeds the equilibrium contribution at $p_T = 4.5$ GeV. Thus with the perturbative estimate of viscosity, the hydrodynamic description breaks down above $p_T \sim 4.5$ GeV. The blast wave model analysis [10], however, indicated that viscous dynamics get invalidated beyond $p_T \sim 1.7$ GeV. The results are not contradictory. In the blast wave model, at the freeze-out, the viscosity is quite large and the sound attenuation length Γ_s is ~ 1.4 fm. In the present simulation, even for the perturbative estimate of viscosity, the sound attenuation length at the freeze-out is $\Gamma_s \sim 0.2$ fm, seven times smaller than the sound attenuation length used in the blast wave analysis. Naturally, nonequilibrium corrections to equilibrium distribution function remain small over an extended p_T range.

We also calculated the elliptic flow in the model. Being a ratio, elliptic flow is very sensitive to the model. Experimentally, elliptic flow saturates at large p_T. It is known that ideal fluid does not explain the saturation of elliptic flow. In contrast to experiment, with ideal fluid elliptic flow continues to increase with p_T. In Fig. 9, we compare the elliptic flow in ideal and viscous fluids. The solid line represents v_2 for the ideal fluid. The long-dashed and medium-dashed lines represent the viscous fluid with ADS/CFT ($\eta/s = 0.08$) and perturbative ($\eta/s = 0.135$) estimated viscosities, respectively. Elliptic flow decreases with viscosity. As viscosity increases, elliptic flow is also reduced. We also note that for both ADS/CFT and perturbative estimates of viscosity, elliptic flow indicates saturation at large p_T. The result is very encouraging, as experimentally elliptic flow also tends to saturate at large p_T.

As discussed earlier, ideal fluid dynamics can explain a large volume of data in Au+Au collisions at RHIC. Our present knowledge about the hot dense matter produced in central Au+Au collisions is obtained from the ideal fluid analysis. As shown in the present article, QGP fluid, even with the ADS/CFT estimate of viscosity $\eta/s = 0.08$, generates enough entropy to enhance particle production by a factor of 3 at $p_T = 3$ GeV. Naturally, if QGP fluid is viscous, initial conditions as required to explain RHIC data with ideal fluid dynamics will overpredict the experimental p_T distribution. Viscous fluid dynamics require an initial temperature much lower than that of an ideal fluid to explain the same p_T spectra. As an example, in Fig. 10, we compare the pion spectra obtained in viscous dynamics with the ADS/CFT estimate of viscosity ($\eta/s = 0.08$), initialized with entropy densities of 110, 80, and 60 fm^{-3}, with the pion spectra obtained in ideal fluid dynamics, initialized with an entropy density of 110 fm^{-3}. For all the fluids, the initial time is $\tau_i = 0.6$ fm and the freeze-out

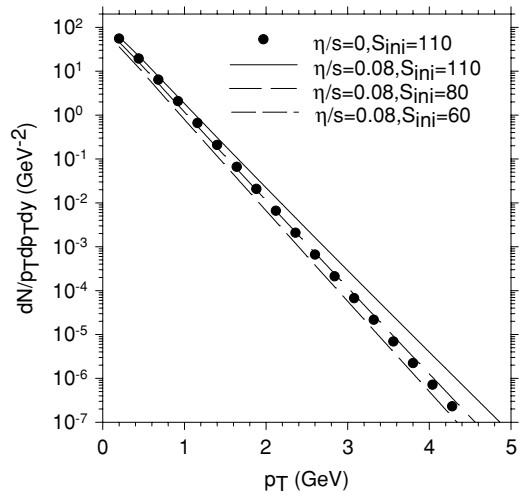

FIG. 10. The solid circles represent the p_T distribution obtained in ideal fluid dynamics, with initial entropy density $s = 110$ fm^{-3}. The solid, long dashed, and dashed lines represent viscous fluid with the ADS/CFT estimate of viscosity, $\eta/s = 0.08$, initialized at entropy density $s = 60$, 80, and 110 fm^{-3}, respectively. Nonequilibrium correction to equilibrium distribution function is included.

temperature is 158 MeV. The viscous fluid initialized with entropy density between 60 and 80 fm^{-3} compares well with the pion spectra from ideal fluid initialized at much higher entropy density. To produce the same pion spectra the ideal fluid requires an initial temperature of 350 MeV while the viscous fluid requires a much lower temperature between 270 and 290 MeV. The ideal fluid dynamics can overestimate the initial temperature of fluid produced in Au+Au collisions at RHIC by 20%–30%.

VII. SUMMARY AND CONCLUSIONS

We studied the boost-invariant hydrodynamic evolution of QGP fluid with dissipation due to shear viscosity. In this study we employed the first-order theory of dissipative relativistic fluid. First-order theories suffer from the problem of causality; the signal can travel faster than light. Unphysical effects, such as reheating of the fluid, can occur early in the evolution. However, for a fluid like QGP, where viscosity is small, with the appropriate initial conditions the effects of causality violation can be minimized. In this model study, we considered two values of viscosity, the ADS/CFT motivated value, $\eta/s \approx 0.08$, and the perturbatively estimated viscosity, $\eta/s \approx 0.135$. Both the ideal and the viscous fluids are initialized similarly. At the initial time $\tau_i = 0.6$ fm, the initial central entropy density is 110 fm^{-3}, with the transverse profile taken from a Glauber model calculation. Viscous hydrodynamics requires initial conditions for the shear stress tensor components. It is assumed that at the equilibration time, the shear stress tensor components have reached their boost-invariant values. The initial conditions of the fluid are such that, for both the values of viscosity ($\eta/s = 0.08$ and 0.135), the condition of validity of viscous hydrodynamics, $\Gamma_s/\tau \ll 1$, is satisfied all through the evolution. Explicit simulation of ideal and viscous fluids confirms that the energy density of a viscous fluid evolves more slowly than its ideal counterpart. The fluid velocities, however, evolve faster in viscous dynamics than in ideal dynamics. Transverse expansion is also greater in viscous dynamics. For a similar freeze-out condition, the freeze-out surface is extended in viscous fluid.

We also studied the effect of viscosity on particle production. Viscosity generates entropy, which leads to enhanced particle production. Particle production is increased because of (i) the extended freeze-out surface and (ii) the nonequilibrium correction to the equilibrium distribution function. The nonequilibrium correction to the equilibrium distribution function is a dominating factor influencing the particle production at large p_T. With the ADS/CFT (perturbative) estimate of viscosity, at $p_T = 3$ GeV, pion production is increased by a factor of 3 (5). The increase is even more at large p_T. While viscosity enhances particle production, it reduces the elliptic flow. At $p_T = 3$ GeV, for the ADS/CFT (perturbative) estimate of viscosity, the elliptic flow is reduced by a factor of 2 (3). We also find that at large p_T the elliptic flow tends to saturate.

To conclude, the present study shows that viscosity, even if small, can be very important in the analysis of RHIC Au+Au collisions. The currently accepted initial temperature of hot dense matter produced in RHIC Au+Au collisions, obtained from ideal fluid analysis, can be changed by 20% or more with dissipative dynamics.

ACKNOWLEDGMENTS

Professor U. Heinz initiated this program of numerical simulation of dissipative hydrodynamics in 2 + 1 dimensions. The author thanks Professor Heinz for several discussions and suggestions.

[1] I. Arsene *et al.* (BRAHMS Collaboration), Nucl. Phys. **A757**, 1 (2005).
[2] B. B. Back *et al.* (PHOBOS Collaboration), Nucl. Phys. **A757**, 28 (2005).
[3] K. Adcox *et al.* (PHENIX Collaboration), Nucl. Phys. **A757**, 184 (2005) [arXiv:nucl-ex/0410003].
[4] J. Adams *et al.* (STAR Collaboration), Nucl. Phys. **A757** (2005) [arXiv:nucl-ex/0501009].
[5] P. F. Kolb and U. Heinz, in *Quark-Gluon Plasma 3*, edited by R. C. Hwa and X.-N. Wang (World Scientific, Singapore, 2004), p. 634.
[6] U. Heinz, J. Phys. G **31**, S717 (2005).
[7] C. Eckart, Phys. Rev. **58**, 919 (1940).
[8] L. D. Landau and E. M. Lifshitz, *Fluid Mechanics* (Pergamon, Oxford, 1963), Sec. 127.
[9] W. Israel, Ann. Phys. (NY) **100**, 310 (1976); W. Israel and J. M. Stewart, *ibid.* **118**, 341 (1979).
[10] D. Teaney, J. Phys. G **30**, S1247 (2004); Phys. Rev. C **68**, 034913 (2003).
[11] A. Muronga, Phys. Rev. Lett. **88**, 062302 (2002) [Erratum **89**, 159901 (2002)]; Phys. Rev. C **69**, 034903 (2004).
[12] A. Muronga and D. H. Rischke, nucl-th/0407114 (v2).
[13] A. K. Chaudhuri and U. Heinz, nucl-th/0504022.
[14] U. Heinz, H. Song, and A. K. Chaudhuri, Phys. Rev. C **73**, 034904 (2006).
[15] K. Kajantie, Nucl. Phys. **A418**, 41 (1984); G. Baym, *ibid.* **A418**, 525 (1984); A. Hosoya and K. Kajantie, *ibid.* **B250**, 666 (1985); A. K. Chaudhuri, J. Phys. G **26**, 1433 (2000); Phys. Scr. **61**, 311 (2000); Phys. Rev. C **51**, R2889 (1995).
[16] R. Baier, P. Romatschke, and U. A. Wiedemann, Phys. Rev. C **73**, 064903 (2006) [arXiv:hep-ph/0602249].
[17] S. R. de Groot, W. A. van Leeuwen, and Ch. G. van Weert, *Relativistic Kinetic Theory* (North-Holland, Amsterdam, 1980), p. 36.
[18] P. Arnold, G. D. Moore, and L. G. Yaffe, J. High Energy Phys. 11 (2000) 001.
[19] G. Baym, H. Monien, C. J. Pethick, and D. G. Ravenhall, Phys. Rev. Lett. **64**, 1867 (1990).
[20] G. Policastro, D. T. Son, and A. O. Starinets, Phys. Rev. Lett. **87**, 081601 (2001).
[21] G. Policastro, D. T. Son, and A. O. Starinets, J. High Energy Phys. **209**, 09 (2002) 043.